Journal of Quantitative Spectroscopy & Radiative Transfer 152 (2015) 107–113

Contents lists available at ScienceDirect

Journal of Quantitative Spectroscopy & Radiative Transfer

journal homepage: www.elsevier.com/locate/jqsrt

Propionaldehyde infrared cross-sections and band strengths

Batikan Köroğlu [a,b], Zachary Loparo [a,b], Janardan Nath [c], Robert E. Peale [c], Subith S. Vasu [a,b,*]

[a] Mechanical and Aerospace Engineering, University of Central Florida, Orlando, FL 32816, USA
[b] Center for Advanced Turbomachinery and Energy Research, University of Central Florida, Orlando, FL 32816, USA
[c] Department of Physics, University of Central Florida, Orlando, FL 32816, USA

ARTICLE INFO

Article history:
Received 5 August 2014
Received in revised form
30 October 2014
Accepted 4 November 2014
Available online 13 November 2014

Keywords:
FTIR
Propionaldehyde
Propanal
Cross-section
Band strength

ABSTRACT

The use of oxygenated biofuels reduces the greenhouse gas emissions; however, they also result in increased toxic aldehyde by-products, mainly formaldehyde, acetaldehyde, acrolein, and propionaldehyde. These aldehydes are carcinogenic and/or toxic and therefore it is important to understand their formation and destruction pathways in combustion and atmospheric systems. Accurate information about their infrared cross-sections and integrated strengths are crucially needed for development of quantitative detection schemes and modeling tools. Critical to the development of such diagnostics are accurate characterization of the absorption features of these species. In this study, the gas phase infrared spectra of propionaldehyde (also called propanal, CH_3–CH_2–CHO), a saturated three carbon aldehyde found in the exhaust emissions of biodiesel or diesel fuels, was studied using high resolution Fourier Transform Infrared (FTIR) spectroscopy over the wavenumber range of 750 – 3300 cm^{-1} and at room temperature 295 K. The absorption cross sections of propionaldehyde were recorded at resolutions of 0.08 and 0.096 cm^{-1} and at seven different pressures (4 – 33 Torr). The calculated band-strengths were reported and the integrated band intensity results were compared with values taken from the Pacific Northwest National Laboratory (PNNL) database (showing less than 2% discrepancy). The peak positions of the 19 different vibrational bands of propionaldehyde were also compared with previous studies taken at a lower resolution of 1 cm^{-1}. To the best of our knowledge, the current FTIR measurements provide the first highest resolution infrared cross section data for propionaldehyde.

1. Introduction

Over the last decade, researchers have examined a variety of biofuels – nearly all of them are oxygenated hydrocarbons – that can be readily blended with fossil fuels [1–4]. However, increased biofuel usage has been linked with increased photochemical smog, cancer mortality, and air pollution concerns due to oxygenated emissions [5–13] and could contribute to more than two million premature mortalities in the world every year [14]. Carbonyl compounds (formaldehyde, acetaldehyde, acrolein, propionaldehyde, and butanone) are listed as hazardous air pollutants (HAP) by the United States Environmental Protection Agency (US EPA report) [15]. Formaldeyhde (CH_2O), acetaldeyhde (CH_3CHO), acrolein (C_3H_4O or C_2H_3CHO), and propionaldehyde (C_2H_5CHO) are reported to be the most abundant aldehydes in the exhaust emissions of biodiesel or diesel fuels [16–20].

There are several chemical kinetic studies [21–23] that compare the modeling and experimental results for the concentration of major and minor species of combustion of

* Corresponding author at: Mechanical and Aerospace Engineering, University of Central Florida, Orlando, FL 32816, USA.
E-mail address: subith@ucf.edu (S.S. Vasu).

http://dx.doi.org/10.1016/j.jqsrt.2014.11.002
0022-4073/

biofuel surrogates. Although the mole fraction profiles of major combustion reaction products (H_2O, CO_2, CO, etc.) and hydrocarbons are reasonably approximated by these mechanisms, the modeling results for the aldehydes do not match with the experimentally obtained values. In addition, the diagnostic methods used in some studies [22] cannot distinguish between acrolein and propionaldehyde and thus give the results as a sum of the two species.

Although there are recently developed laser absorption schemes in the literature [24] for the detection of the formaldehyde and acetaldehyde in a shock tube combustion reaction, there is no study to the best of our knowledge on the interference free detection of acrolein or propionaldehyde using laser absorption spectrocopy in a combustion environment. Critical to the development of such diagnostics is the accurate characterization of the absorption features of these aldehydes. The absorption cross section of acrolein, propionaldehyde, and acetaldehyde are available in the PNNL database at atmopsheric pressure and at three different temperatures (5, 25, and 50 °C) [25]. The formaldehyde spectrum can be obtained from the HITRAN database [26]. Figs. 1(a) and 1(b) show the spectra for these four species at 296 K in 1650–1850 cm^{-1} and 2600–3100 cm^{-1}, respectively. These four aldehydes share the same carbonyl group C=O vibrational stretching which gives rise to the absorption transition between 1710 and 1740 cm^{-1}. In addition, the common (C–H) bond found in the aldehydes results in transitions between 2690 and 2840 cm^{-1}. During

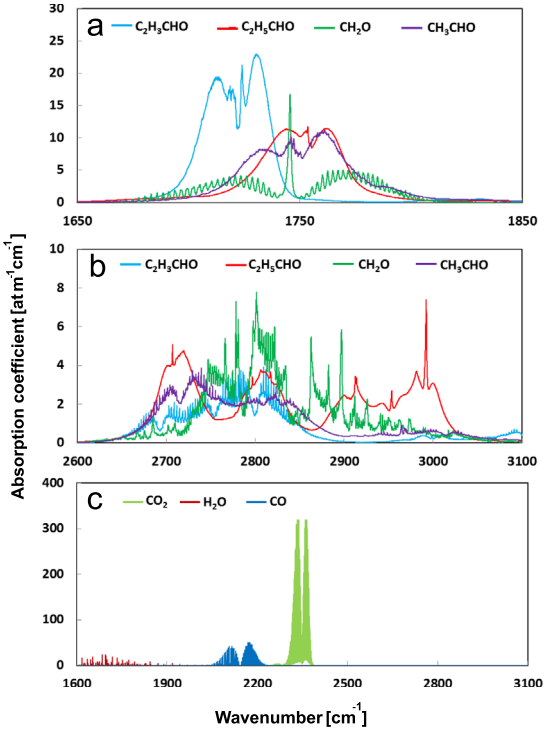

Fig. 1. Absorption spectra of (a), (b) aldehydes: acrolein (C_2H_3CHO), propionaldehyde (C_2H_5CHO), formaldehyde (CH_2O), and acetaldehyde (CH_3CHO); and (c) interfering species: carbon dioxide (CO_2), water (H_2O), and carbon monoxide (CO). Data is taken from PNNL and HITRAN databases.

combustion of fuels, other intermediates also form and they also have absorption features in the infrared (IR) region. Fig. 1(c) shows the spectra of CO_2, H_2O, and CO within 1650–3100 cm^{-1}. Although, neither CO_2 nor CO has any common features with the aldehydes in the mid IR, H_2O is a possible interfering species in the development of laser absorption scheme for the aldehydes. Therefore, it is important to accurately determine the spectral parameters such as absorption cross sections, line strengths, and broadening coefficients of the aldehydes so that calibration free sensors could be developed for the species of interest.

In the literature, there are some studies on the microwave [27,28] and infrared [29–33] spectra of propionaldehyde. The fundamental vibrational band assignments were conducted for normal propionaldehyde (propanaldehyde-d0) as well as its three isotopomers (propionaldehyde-d1, d2, and d5). One of the most recent studies was conducted by Guirgis et al. [29] in which they recorded the mid IR spectrum of propionaldehyde from 400 to 3500 cm^{-1} at resolution of 1 cm^{-1} and the far IR spectrum of propionaldehyde from 50 to 360 cm^{-1} at resolution of 0.1 cm^{-1}. They reported the 24 fundamental vibrational bands and also indicated the discrepancies with previous studies in the assignments of 6 of the fundamentals. Also, they performed ab initio calculations and reassigned some of these bands with the help of the IR and Raman data taken for gaseous, liquid, and solid propionaldehyde.

In this study a Fourier Transform Infrared Spectrometer (FTIR) is used to determine the absorption cross section of propionaldehyde as well as its band strengths in the wavenumber regions between 750 and 3300 cm^{-1}. In order to accurately determine the cross section of propionaldehyde, the measurements were carried out at room temperature (295 K) and at seven different pressures (6, 8, 10, 12, 14, 22, and 33 Torr). The absorption cross section was recorded at resolutions of 0.08 and 0.096 cm^{-1} for the wavenumber regions from 750 to 1900 cm^{-1} and 1900 to 3300 cm^{-1}, respectively. The results were compared with the spectral data of PNNL database taken at a temperature of 296 K and resolution of 0.112 cm^{-1} [25]. The integrated band intensities were calculated to compare the current study results with the PNNL database. The current study results also give the 19 fundamental frequencies that fall within 750–3300 cm^{-1} and the assignments shown here are based on the previous works of Guirgis et al. [29].

2. Experimental setup and procedure

The absorption spectra of propionaldehyde was recorded over the wavenumber range of 750–3300 cm^{-1} using a vacuum bench Bomem DA8 Fourier Transform Infrared spectrometer (see for details, Ref. [34]). Fig. 2 shows the schematic of the current FTIR setup. The spectrometer has a maximum resolution of 0.017 cm^{-1}. In this study the highest useful resolution was 0.08 cm^{-1} due to the relatively broad linewidth feature of the analyte [25]. The FTIR was configured as described in Table 1. A potassium bromide (KBr) beam splitter was used with the globar light source to make the measurements along a 10 cm path length stainless steel cell with NaCl windows.

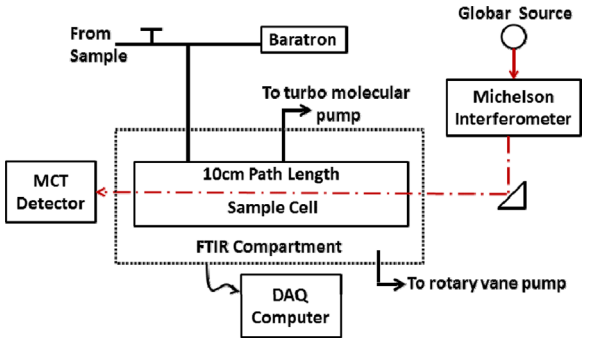

Fig. 2. Experimental setup for the FTIR measurements of propionaldehyde.

Table 1
FTIR configuration for the measurements of Propionaldehyde spectroscopic parameters.

FTIR spectrometer configuration	
Resolution	0.08 and 0.096 cm^{-1}
Beamsplitter	Potassium bromide (KBr)
FTIR input aperture	3.5 mm
Detector	MCT HgCdTe
Lightsource	Globar (mid-infrared)
Optical path length (stainless-steel cell)	10 cm
Zero-filling	2 × and 4 × zero-filling
Pressure gauge	Baratron (1000 Torr FSR, ±0.05% accuracy)

An MCT detector was used for the spectral measurements. With these resources, the wavenumber range was 400–6500 cm^{-1}. Pressure in the sample cell was monitored using a Baratron capacitance gauge (1000 Torr full-scale range, 0.05% uncertainty). The manifold and the sample cell, located inside the FTIR compartment, were evacuated to less than 1×10^{-5} Torr with a turbo molecular pump system (Edwards T11213302) before the start of every experiment. The FTIR chamber was evacuated to pressures of less than 0.1 Torr with a rotary vane pump in order to minimize the interference by atmospheric air. The average leak rate of the cell was 3.0×10^{-3} Torr/min. The spectral measurements were carried out at seven different pressures (6, 8, 10, 12, 14, 22, and 33 Torr) and at room temperature (295 K) to accurately determine the absorption cross section and the band strength. To account for the spectral drift in the data, reference scans were taken before and after the transmission data. This drift was taken into account in determining the uncertainty of propionaldehyde absorption cross section. Interference from H_2O or CO_2 lines divided out, so that they were not observed in the measured transmittance spectra.

A spectrometer aperture size of 3.5 mm was chosen with 300 coadded interferometer scans to obtain the desired spectral resolution with adequate signal-to-noise ratio (SNR). The data within the regions of 750–1900 cm^{-1} and 1900–3300 cm^{-1} were taken at 0.08, and 0.096 cm^{-1} resolution, respectively. The interferograms were zero filled by a factor of 2 for the 0.096 cm^{-1} resolution scans and by a factor of 4 for the 0.08 cm^{-1} resolution scans to obtain smoother line profiles. The high resolution spectra were taken at these spectral regions because all the aldehydes have strongly absorbing features due to their common C–O and C–H stretching. High purity propionaldehyde (> 99.6%), supplied by Fisher Scientific, was used in this study. Samples were prepared by transferring the propionaldehyde into a glass test tube that was connected to the all-stainless-steel gas-handling manifold via a Swagelok Ultra-Torr vacuum fitting.

3. Data analysis

3.1. Absorption cross-section of propionaldehyde

The rotational and vibrational transitions of the gas molecules through absorption of the incident light at frequency, ν follow the Beer Lambert law given by

$$-\ln\left(I/I_o\right)_\nu = S\phi_\nu PL = \beta_\nu PL = \alpha_\nu \tag{1}$$

where I and I_o are the spectral intensity of the light passing through the analyte propionaldehyde and the empty cell, respectively; S [$cm^{-2}\,atm^{-1}$] is the line strength; ϕ_ν [cm] is the frequency-dependent lineshape function; β_ν [$cm^{-1}\,atm^{-1}$] is the frequency-dependent absorption coefficient; P [atm] is the pressure of the gas inside the cell; L [cm] is the optical path length; and α_ν is the absorbance.

The integrated absorbance removes the normalized contribution of the lineshape and thus reduces Eq. (1) to

$$A = \int \alpha_\nu \, d\nu = S_{band} PL \tag{2}$$

The integrated absorbance given by Eq. (2) was plotted in Fig. 4 for different bands of propionaldehyde to show the linearity of the integrated absorbance with the product, PL, and thus to obtain the S_{band} through the slope of the linear fit.

3.2. Comparison of current study results with PNNL database

To compare the current study results with those from PNNL [25], the dependence of absorption coefficient on temperature and pressure must be eliminated. Therefore, the absorption cross-section σ_ν [cm^2/molecule] is used for comparison purposes, which can be obtained through the knowledge of β_ν as follows:

$$\sigma_\nu = \left(\frac{T}{273.15}\right)\left(\frac{\beta_\nu}{N}\right) \tag{3}$$

where T [K] is the temperature of the gas and $N=2.6867\times10^{19}$ [molecule/cm^3 atm] is the Loschmidt number at standard temperature (273.15 K) and pressure (1 atm).

The PNNL data was recorded at a total pressure of 1 atm with 10 different propionaldehyde mole fractions in pure N_2 at 296 K [25]. The optical path length of the cell was 100 cm. These values were used in Eqs. (1) and (3) to obtain the σ_ν values of propionaldehyde from PNNL. In this study, the absorption spectrum was recorded at seven different pressures to accurately determine the absorption

cross sections [σ_ν]. A data reduction scheme described by Sharpe et al. [25] was used to report the PNNL database and subsequently was implemented in the current work to compare our results with those of PNNL. In this scheme, the recorded absorbance [A] from each different pressure measurement was plotted against the burden [PL], defined as the pressure [P] multiplied by the optical path length [L]. A weighted least squares fit with zero intercept was then performed in which the data points with an absorbance of $\alpha_\nu \geq 1.6$ were assigned a weight of zero. The slope of the fit was the absorption coefficient [β_ν] given in Eq. (1). The weighting scheme favors higher burden measurements for weakly absorbing features and lower burden measurements for strongly absorbing features. The main reason for applying this scheme was to remove the transmission data points which show saturation at certain wavenumbers due to the strong absorption of propionaldehyde. The overall effect of this fit is to reduce the inherent nonlinearities of the FTIR measurements and also to improve the SNR.

4. Results and discussion

4.1. Absorption cross-section and vibrational assignments

Fig. 3 shows the current study results of the absorption cross-section of propionaldehyde (CH_3–CH_2–CHO) as well as the vibrational assignments for different spectral regions of interest at room temperature (295 K). Fig. 3 also includes the data of PNNL taken at 296 K for comparison purposes. The spectra shown in Fig. 3(a–c) were recorded at 0.08 cm^{-1} resolution, whereas Fig. 3(d) data was recorded at 0.096 cm^{-1} resolution. Fig. 3 demonstrates that the discrepancy between the current study results and PNNL database is very small. The exact difference is given in the next section; however, it is clear from the figure that the sharp rovibrational Q transitions have higher absorption cross sections in the current study than those given by PNNL database. The difference becomes more pronounced especially for ν_7, ν_{13}, and ν_{16} transitions. This result is attributed to the fact that the spectral lines are better resolved in the present study. Propionaldehyde shows strong absorption bands in the mid IR region. Various vibrational modes of propionaldehyde given in Fig. 3 were based on the assignments of previous study by Guirgis et al. [29] which recorded the spectrum at 1 cm^{-1}

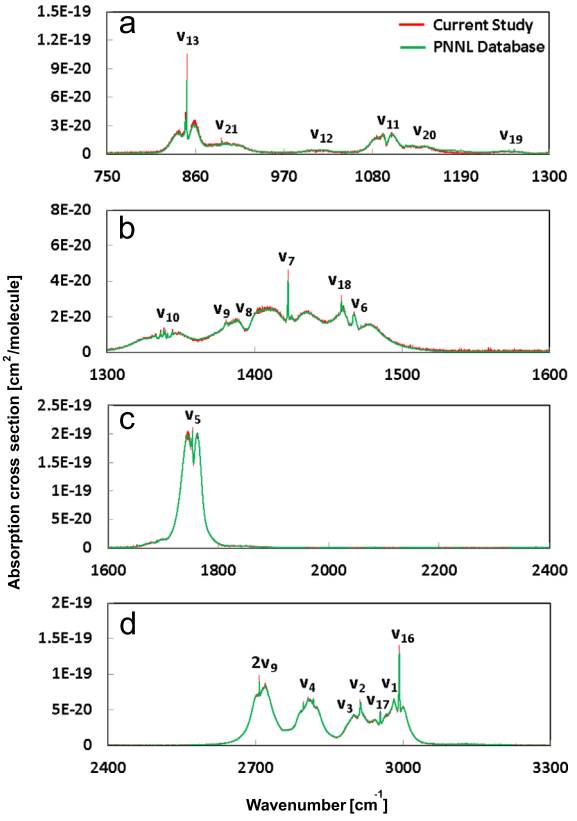

Fig. 3. IR absorption spectra of propionaldehyde at 295 K in the regions of (a) 750–1300 cm^{-1}, (b) 1300–1600 cm^{-1}, (c) 1600–2400 cm^{-1}, (d) 2400–3300 cm^{-1}.

Table 2
Vibrational assignments for the IR bands of propionaldehyde.

Band	Fundamental wavenumber [cm^{-1}] (Guirgis et al.)	Fundamental wavenumber [cm^{-1}] (current study)	Vibrational assignment
$\nu_1(a')$	2981	2980.83	CH_3 antisymmetric stretch
$\nu_2(a')$	2914	2913.88	CH_2 symmetric stretch
$\nu_3(a')$	2905	2905.80	CH_3 symmetric stretch
$\nu_4(a')$	2818	2817.60	CH stretch
$\nu_5(a')$	1754	1753.57	C–O stretch
$\nu_6(a')$	1467	1467.42	CH_3 antisymmetric deformation
$\nu_7(a')$	1423	1422.71	CH_2 deformation
$\nu_8(a')$	1395	1394.75	CH_3 symmetric deformation
$\nu_9(a')$	1381	1380.49	CH bend
$\nu_{10}(a')$	1339	1338.49	CH_2 wag
$\nu_{11}(a')$	1098	1098.33	CH_3 rock
$\nu_{12}(a')$	1009	1009.71	CCC antisymmetric stretch
$\nu_{13}(a')$	849	849.14	CCC symmetric stretch
$\nu_{14}(a')$	661	–	OCC bend
$\nu_{15}(a')$	264.1	–	CCC bend
$\nu_{16}(a'')$	2992	2992.28	CH_3 antisymmetric stretch
$\nu_{17}(a'')$	2954	2953.53	CH_2 antisymmetric stretch
$\nu_{18}(a'')$	1459	1458.87	CH_3 antisymmetric deformation
$\nu_{19}(a'')$	1250	1249.96	CH_2 twist
$\nu_{20}(a'')$	1127	1127.29	C–H bend
$\nu_{21}(a'')$	892	891.95	CH_3 rock
$\nu_{22}(a'')$	658	–	CH_2 rock
$\nu_{23}(a'')$	219.9	–	Methyl torsion
$\nu_{24}(a'')$	135.1	–	C(O)H torsion

resolution using Fourier Transform Spectrometer from 400 to 3500 cm^{-1} and at 0.1 cm^{-1} resolution from 50 to 380 cm^{-1}.

Propionaldehyde has 24 vibrational modes. Table 2 shows the positions of these fundamental bands and the vibrational assignments based on the results of the current study and those of Guirgis et al. [29]. There are mainly two vibrational modes of propionaldehyde which are common to all the aldehydes. These are the very strong C–O stretch and the strong C–H stretch. The very strong C–O stretch of propionaldehyde is assigned as the ν_5 band. It has the three main peaks (*P*, *Q*, and *R* rotational lines) and is centered at 1753.57 cm^{-1}. The strong CH stretch of propionaldehyde is centered at 2817.60 cm^{-1} and is assigned as the ν_4 band. In the 750–1290 cm^{-1} spectral region, propionaldehyde has also a very strong CCC symmetric stretch assigned as the ν_{13} band. In this region, there are other weaker vibrational modes, ν_{21}, ν_{12}, ν_{11}, ν_{20}, and ν_{19}. In the 1290–1530 cm^{-1} spectral region, the relatively strong ν_7 band centered at 1422.71 cm^{-1} involves CH_2 deformation. In the 2650–3050 cm^{-1} spectral range, there is a very strong CH_3 antisymmetric stretch at 2992.28 cm^{-1}. Note that the current study results do not include five of the fundamentals (ν_{14}, ν_{15}, ν_{22}, ν_{23}, and ν_{24}) that fall in the far IR region, because the MCT detector is unusable below 500 cm^{-1}. Even between 500 and 750 cm^{-1} the SNR for the given spectrometer resources was relatively low. A lower resolution of ~0.25 cm^{-1} was needed to obtain adequate SNR below 500 cm^{-1}. However, this range of data is not included here.

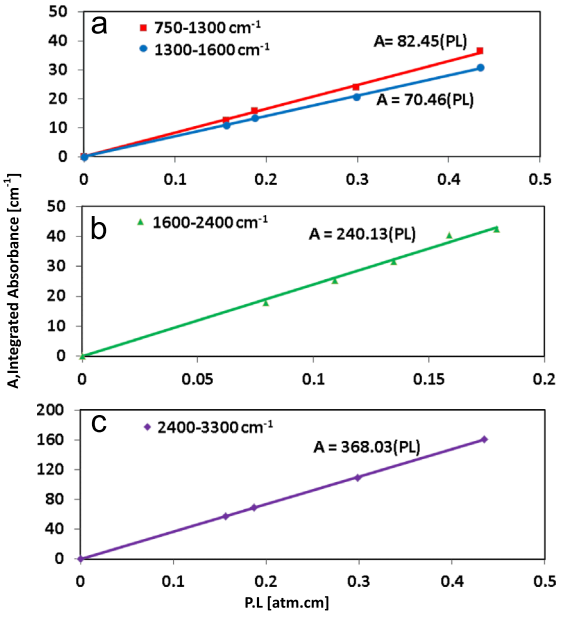

Fig. 4. Linear dependence of integrated absorbance on PL for various IR bands.

4.2. Integrated absorbance and band strengths of propionaldehyde and comparison with PNNL data

The absorption spectrum was divided into four different regions, (750–1300 cm^{-1}), (1300–1600 cm^{-1}), (1600–2400 cm^{-1}), and (2400–3300 cm^{-1}). The integrated absorbance, [*A*], given by Eq. (2) was calculated for each spectral region. The integrated absorbance values for each region were then plotted against the burden [*P.L*]. A linear regression line with zero intercept was fit to each region. The results are presented in Fig. 4. The fits for each of the regions had a correlation coefficient of $R \sim 0.99$. The linear behavior of the integrated absorbance for each spectral region indicates that the intensities did not approach saturation and thus the Beer–Lambert law was applicable. The slope of the fitted line is the band strength, S_{band}, and is reported for each of the spectral regions in Table 3.

The absorption cross section data of propionaldehyde obtained in this study has a higher wavenumber resolution than the PNNL database. The PNNL data was recorded at 0.112 cm^{-1}, whereas the current study results were recorded at 0.08 cm^{-1} within 750–1900 cm^{-1} and at 0.096 cm^{-1} within 1900–3300 cm^{-1}. Therefore, a comparison approach as described in Es-sebbar et al. [35] was used, in which the integrated IR cross sections ($\int \sigma_\nu \, d\nu$) of propionaldehyde, rather than the absorption cross section at each wavenumber, were calculated and compared between the current study results and PNNL database. The comparison results are also outlined in Table 3. There was a very good agreement between the current experimental data results and PNNL database, the maximum deviation being 1.96% for the 1300–1600 cm^{-1} region. The difference between the two measurements decreased as the wavenumber is increased and was only 0.25% in the 2400–3300 cm^{-1} region.

4.3. Uncertainty

Based on Eqs. (1)–(3) there is uncertainty in the calculation of absorption cross section [σ_ν], band strength [S_{band}], and integrated intensity [$\int \sigma_\nu \, d\nu$] due to the errors

Table 3
The band strengths of propionaldehyde at various infrared regions and comparison of integrated absorption cross sections between PNNL database and current study.

Wavenumber [cm^{-1}]	Current study		PNNL	% Difference
	S_{band} [cm^{-2} atm^{-1}]	$\int \sigma_\nu \, d\nu$ [cm/molecule]	$\int \sigma_\nu \, d\nu$ [cm/molecule]	
750–1300	82.45	3.30×10^{-18}	3.35×10^{-18}	−1.27
1300–1600	70.46	2.72×10^{-18}	2.77×10^{-18}	−1.96
1600–1900	240.13	9.87×10^{-18}	9.70×10^{-18}	1.75
2400–3300	368.03	1.49×10^{-17}	1.49×10^{-17}	0.25

Table 4
Uncertainty analysis results for the absorption cross section, band strength, and integrated intensity of propionaldehyde.

		Wavenumber range [cm^{-1}]			
		750–1300	1300–1600	1600–2400	2400–3300
Measured variables	P [atm]	$\pm 0.05\%$			
	T [K]	± 0.5 °C			
	α_ν	$\pm 9.15\%$	$\pm 4.71\%$	$\pm 0.03\%$	$\pm 0.87\%$
Calculated variables	σ_ν[cm^2/molecule]	$\pm 9.15\%$	$\pm 4.72\%$	$\pm 0.18\%$	$\pm 0.93\%$
	S_{band} [cm^{-2} atm^{-1}]	$\pm 4.21\%$	$\pm 3.41\%$	$\pm 0.74\%$	$\pm 2.85\%$
	$\int \sigma_\nu d\nu$[cm/molecule]	$\pm 6.11\%$	$\pm 3.58\%$	$\pm 4.23\%$	$\pm 2.95\%$

in the measurements of pressure [P], temperature [T], and absorbance [α_ν]. The uncertainty of the pressure measurement resulted from the Baratron pressure gauge, which has an accuracy of 0.05%, as well as from the variation in the pressure of the sample cell due to the adsorption of molecules on the cell walls. The room temperature measurement had an uncertainty of ± 0.5 °C. The reference (vacuum) spectra were collected before and after the sample measurements to account for the drift of the signal. Table 4 shows the results of the uncertainty analysis for different wavenumber regions of the spectra. The background measurement drift was the main source of error that contributed to the uncertainty of the absorbance. The maximum uncertainty in the cross section was estimated to be $\pm 9.15\%$, which occurred for lower wavenumber regions (750–1300 cm^{-1}) where the absorption of the propionaldehyde was very small. The maximum uncertainty in the other wavenumber regions was smaller. Note that the uncertainty varies by wavenumber; therefore, the resulting maximum uncertainty in the band strength and integrated intensity are weighted averages of the uncertainties in the cross section calculation.

5. Conclusions

The current study used a high-resolution Fourier Transform Infrared Spectrometer to measure the IR absorption cross-sections of propionaldehyde at room temperature (295 K) and at spectral resolutions of 0.08 and 0.096 cm^{-1} within the spectral regions of 750–1900 cm^{-1} and 1900–3300 cm^{-1}, respectively. The absorption spectra as well as the fundamental line positions were presented. The band strengths were reported for various spectral regions and the integrated band intensities were compared with the PNNL database, which were recorded at a lower resolution of 0.112 cm^{-1}. There was a very good agreement between the current experimental data results and PNNL database, the maximum deviation being 1.9645% for the 1300–1600 cm^{-1} region. The difference between the two measurements decreased as the wavenumber is increased and was only 0.25% in the 2400–3300 cm^{-1} region. Since the spectral lines were better resolved, the rovibrational Q transitions had higher absorption cross sections in the present study than those given by PNNL database. This study will aid in the development of quantitative absorption detection schemes for the concentration measurement of propionaldehyde, a major biofuel combustion intermediate which is also exhausted, and the results can be readily incorporated in atmospheric models.

Acknowledgments

Research at UCF was supported by financial assistance from the Mechanical and Aerospace Department and the Office of Research and Commercialization. The authors thank Chris Fredricksen for useful discussions and help with the setup.

References

[1] Yang Y, Dec JE Bio-Ketones: autoignition characteristics and their potential as fuels for HCCI engines. SAE technical paper 2013-01-2627; 2013.
[2] Barari G, Koroglu B, Vasu SS, Dec JE, Taatjes CA. HCCI engine modeling of diisopropyl ketone, a prototypical biofuel. ESS fall technical meeting. Clemson, SC; 2013.
[3] Badra J, Elwardany A, Khaled F, Vasu SS, Farooq A. A shock tube and laser absorption study of ignition delay times and OH reaction rates of ketones: 2-butanone and 3-buten-2-one. Combust Flame 2014;161(3):725–34.
[4] Allen JW, Scheer AM, Gao CW, Merchant SS, Vasu SS, Welz O, et al. A coordinated investigation of the combustion chemistry of diisopropyl ketone, a prototype for biofuels produced by endophytic fungi. Combust Flame 2014;161:711–24.
[5] Ginnebaugh DL, Liang J, Jacobson MZ. Examining the temperature dependence of ethanol (E85) versus gasoline emissions on air pollution with a largely-explicit chemical mechanism. Atmos Environ 2010;44:1192–9.
[6] Jacobson MZ. Effects of biofuels vs. other new vehicle technologies on air pollution, global warming, land use and water. Int J Biotechnol 2009;11:14–59.
[7] Jacobson MZ. Short-term effects of controlling fossil-fuel soot, biofuel soot and gases, and methane on climate, Arctic ice, and air pollution health. J Geophys Res D: Atmos 2010;115(4).
[8] Jacobson MZ. Effects of ethanol (E85) versus gasoline vehicles on cancer and mortality in the United States. Environ Sci Technol 2007;41:4150–7.
[9] Gaffney JS, Marley NA. The search for clean alternative fuels: there's no such thing as a free lunch!. Atmos Environ – Part A Gen Top 1990;24:3105–7.
[10] Gaffney JS, Marley NA. Comment on environmental implications on the oxygenation of gasoline with ethanol in the metropolitan area of Mexico City. Environ Sci Technol 2001;35:4957–60.
[11] Gaffney JS, Marley NA. The impacts of combustion emissions on air quality and climate – from coal to biofuels and beyond. Atmos Environ 2009;43:23–36.
[12] Gaffney JS, Marley NA, Blake DR. Baseline measurements of ethene in 2002: implications for increased ethanol use and biomass burning on air quality and ecosystems. Atmos Environ 2012;56:161–8.
[13] Gaffney JS, Marley NA, Martin RS, Dixon RW, Reyes LG, Popp CJ. Potential air quality effects of using ethanol–gasoline fuel blends: a field study in Albuquerque, New Mexico. Environ Sci Technol 1998;31:3053–61.

[14] Silva RA, West JJ, Zhang Y, Anenberg SC, Lamarque J-F, Shindell DT, et al. Global premature mortality due to anthropogenic outdoor air pollution and the contribution of past climate change. Environ Res Lett 2013;8(3):034005.
[15] US EPA report. Available at 〈http://www2.epa.gov/regulatory-information-topic/air#transport〉, accessed 10/1/2014.
[16] Chai M, Lu M, Liang F, Tzillah A, Dendramis N, Watson L. The use of biodiesel blends on a non-road generator and its impacts on ozone formation potentials based on carbonyl emissions. Environ Pollut 2013;178:159–65.
[17] Karavalakis G, Boutsika V, Stournas S, Bakeas E. Biodiesel emissions profile in modern diesel vehicles. Part 2: effect of biodiesel origin on carbonyl, PAH, nitro-PAH and oxy-PAH emissions. Sci Total Environ 2011;409:738–47.
[18] Guarieiro LLN, PAdP Pereira, Torres EA, da Rocha GO, de Andrade JB. Carbonyl compounds emitted by a diesel engine fuelled with diesel and biodiesel–diesel blends: sampling optimization and emissions profile. Atmos Environ 2008;42:8211–8.
[19] Fontaras G, Karavalakis G, Kousoulidou M, Ntziachristos L, Bakeas E, Stournas S, et al. Effects of low concentration biodiesel blends application on modern passenger cars. Part 2: Impact on carbonyl compound emissions. Environ Pollut 2010;158:2496–503.
[20] Guarieiro LLN, de Souza AF, Torres EA, de Andrade JB. Emission profile of 18 carbonyl compounds, CO, CO_2, and NO_x emitted by a diesel engine fuelled with diesel and ternary blends containing diesel, ethanol and biodiesel or vegetable oils. Atmos Environ 2009;43:2754–61.
[21] Glaude PA, Herbinet O, Bax S, Biet J, Warth V, Battin-Leclerc F. Modeling of the oxidation of methyl esters—validation for methyl hexanoate, methyl heptanoate, and methyl decanoate in a jet-stirred reactor. Combust Flame 2010;157:2035–50.
[22] Biet J, Hakka MH, Vr Warth, Glaude P-A, Battin-Leclerc FDR. Experimental and modeling study of the low-temperature oxidation of large alkanes. Energy Fuels 2008;22:2258–69.
[23] Liu D, Togbé C, Tran L-S, Felsmann D, Oßwald P, Nau P, et al. Combustion chemistry and flame structure of furan group biofuels using molecular-beam mass spectrometry and gas chromatography – Part I: Furan. Combust Flame 2014;161:748–65.
[24] Wang S, Davidson DF, Hanson RK. High-temperature laser absorption diagnostics for CH_2O and CH_3CHO and their application to shock tube kinetic studies. Combust Flame 2013;160:1930–8.
[25] Sharpe SW, Johnson TJ, Sams RL, Chu PM, Rhoderick GC, Johnson PA. Gas-phase databases for quantitative infrared spectroscopy. Appl Spectrosc 2004;58:1452.
[26] Rothman LS, Gordon IE, Babikov Y, Barbe A, Chris Benner D, Bernath PF, et al. The HITRAN2012 molecular spectroscopic database. J Quant Spectrosc Radiat Transf 2013;130:4–50.
[27] Randell J, Hardy JA, Cox AP. The microwave spectrum and potential function of propanal. J Chem Soc Faraday Trans 2 1988;84:1199–212.
[28] Pickett HM. Microwave spectrum and internal rotation potential of propanal. J Chem Phys 1974;61:3954.
[29] Guirgis GA, Drew BR, Gounev TK, Durig JR. Conformational stability and vibrational assignment of propanal. Spectrochim Acta Part A: Mol Biomol Spectrosc 1998;54:123–43.
[30] Durig JR, Compton DAC, McArver AQ. Low frequency vibrational spectra, methyl torsional potential functions, and internal rotational potential of propanal. J Chem Phys 1980;73:719.
[31] Durig JR, Guirgis GA, Bell S, Brewer WE. Far-infrared spectrum, ab initio calculations, conformational energy differences, barriers to internal rotation and r0 structure of propanal. J Phys Chem A 1997;101:9240–52.
[32] Frankiss SG, Kynaston W. The vibrational spectra of propanal, 1-deuteropropanal and 2,2-dideuteropropanal. Spectrochim Acta Part A: Mol Spectrosc 1972;28:2149–61.
[33] Sbrana G, Schettino V. Vibrational spectra and isomerism in propyl- and butylaldehydes. J Mol Spectrosc 1970;33:100–8.
[34] Peale RE, Muravjov AV, Fredricksen CJ, Boreman GD, Saxena H, Braunstein G, et al. Spectral signatures of acetone vapor from ultraviolet to millimeter wavelengths. In: Proceedings of the International Symposium on Spectral Sensing Research, Bar Harbour, ME; June 2006.
[35] Es-sebbar E-T, Alrefae M, Farooq A. Infrared cross-sections and integrated band intensities of propylene: temperature-dependent studies. J Quant Spectrosc Radiat Transf 2014;133:559–69.